BIOCHEMISTRY
including biophysical chemistry & molecular biology

Article

pubs.acs.org/biochemistry

Structural Evidence of a Productive Active Site Architecture for an Evolved Quorum-Quenching GKL Lactonase

Bo Xue,[†] Jeng Yeong Chow,[‡] Amgalanbaatar Baldansuren,[§] Lai Lai Yap,[‡] Yunn Hwen Gan,[‡] Sergei A. Dikanov,[§] Robert C. Robinson,*[,†,‡,∥] and Wen Shan Yew*[,‡]

[†]Institute of Molecular and Cell Biology, 61 Biopolis Drive, Singapore 138673

[‡]Department of Biochemistry, Yong Loo Lin School of Medicine, National University of Singapore, 8 Medical Drive, Singapore 117597

[§]Department of Veterinary Clinical Medicine, University of Illinois at Urbana-Champaign, Urbana, Illinois 61801, United States

[∥]School of Biological Sciences, Nanyang Technological University, 60 Nanyang Drive, Singapore 637551

Supporting Information

ABSTRACT: The in vitro evolution and engineering of quorum-quenching lactonases with enhanced reactivities was achieved using a thermostable GKL enzyme as a template, yielding the E101G/R230C GKL mutant with increased catalytic activity and a broadened substrate range [Chow, J. Y., Xue, B., Lee, K. H., Tung, A., Wu, L., Robinson, R. C., and Yew, W. S. (2010) *J. Biol. Chem.* *285*, 40911−40920]. This enzyme possesses the $(\beta/\alpha)_8$-barrel fold and is a member of the PLL (phosphotriesterase-like lactonase) group of enzymes within the amidohydrolase superfamily that hydrolyze *N*-acyl-homoserine lactones, which mediate the quorum-sensing pathways of bacteria. The structure of the evolved *N*-butyryl-L-homoserine lactone (substrate)-bound E101G/R230C GKL enzyme was determined, in the presence of the inactivating D266N mutation, to a resolution of 2.2 Å to provide an explanation for the observed rate enhancements. In addition, the substrate-bound structure of the catalytically inactive E101N/D266N mutant of the manganese-reconstituted enzyme was determinied to a resolution of 2.1 Å and the structure of the ligand-free, manganese-reconstituted E101N mutant to a resolution of 2.6 Å, and the structures of ligand-free zinc-reconstituted wild-type, E101N, R230D, and E101G/R230C mutants of GKL were determinied to resolutions of 2.1, 2.1, 1.9, and 2.0 Å, respectively. In particular, the structure of the evolved E101G/R230C mutant of GKL provides evidence of a catalytically productive active site architecture that contributes to the observed enhancement of catalysis. At high concentrations, wild-type and mutant GKL enzymes are differentially colored, with absorbance maxima in the range of 512−553 nm. The structures of the wild-type and mutant GKL provide a tractable link between the origins of the coloration and the charge-transfer complex between the α-cation and Tyr99 within the enzyme active site. Taken together, this study provides evidence of the modulability of enzymatic catalysis through subtle changes in enzyme active site architecture.

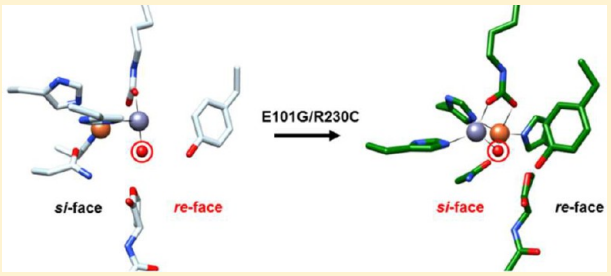

Quorum sensing is an integral part of microbial interaction and is responsible for mediating virulence of pathogenic bacteria.[1] Quorum quenching, an attenuation of the quorum-sensing pathway, has been shown to be an effective antivirulence strategy.[2] We are interested in developing quorum-quenching lactonases as antivirulence therapeutic agents to modulate quorum-sensing pathways of disease-causing microbes. Previously, we reported the in vitro evolution of a thermostable GKL (quorum-quenching lactonase from *Geobacillus kaustophilus*) enzyme with increased catalytic efficiencies and a broadened substrate range.[3] This GKL enzyme is part of a group of phosphotriesterase-like lactonases (PLLs) that hydrolyze quorum-sensing *N*-acyl-homoserine lactones (AHLs);[4,5] members of this group are divergently related to other enzymes of the amidohydrolase superfamily.

The amidohydrolase superfamily is a homologous group of enzymes that catalyze hydrolytic reactions on a broad range of substrates bearing ester or amide functional groups with carbon or phosphorus centers.[6] Members of the superfamily bear a conserved mononuclear or binuclear metal center within a $(\beta/\alpha)_8$-barrel structural scaffold.[7] This metal center is involved in the activation of a water molecule for subsequent nucleophilic attack on an activated scissile bond of the substrate; resolution of the reaction intermediate results in subsequent hydrolysis.

In our attempts to understand the basis for the observed rate enhancements (and broadened substrate range) of the evolved E101G/R230C GKL mutant (the mutations are localized on loops at the C-terminal ends of the third and seventh β-strands, respectively), especially toward the hydrolysis of *N*-butyryl-L-homoserine lactone (C4-HSL, a substrate that wild-type GKL

Received: January 24, 2013
Revised: March 3, 2013
Published: March 5, 2013

   dx.doi.org/10.1021/bi4000904 | *Biochemistry* 2013, 52, 2359−2370

previously could not hydrolyze), the structure of the evolved mutant was determined in the presence of C4-HSL bound in the enzyme active site and the inactivating D266N mutation. This report provides structural evidence of a catalytically competent active site architecture to account for the catalytic enhancements observed in the evolved mutant. Our study also suggests that the productive geometry of the enzyme active site can be positively modulated through subtle changes (suitable point mutations), reinforcing the need to consider the interplay between active site architecture and catalysis in future enzyme design and engineering efforts.

MATERIALS AND METHODS

The substrates *N*-butyryl-DL-homoserine lactone (C4-HSL), *N*-(3-oxohexanoyl)-L-homoserine lactone (3-oxo-C6-HSL), and *N*-(3-oxooctanoyl)-L-homoserine lactone (3-oxo-C8-HSL) were purchased from Sigma-Aldrich Co. (St. Louis, MO). All reagents were the highest quality grade commercially available.

Expression and Protein Purification of Wild-Type GKL and Its Mutants. Wild-type GKL and its mutants were expressed and purified as previously described,[3] with the following modifications. Briefly, the His-tagged proteins were expressed in *Escherichia coli* strain BL21(DE3) in LB supplemented with 100 μg/mL ampicillin; when the cells were grown to an OD_{600} of 0.1, 0.1 mM 2′-2-bipyridal (Sigma) was added to the culture. The culture was grown to an OD_{600} of 0.6, and 0.1 mM IPTG was added for induction for an additional 16 h at 37 °C. The cells were harvested, and the protein was purified by affinity chromatography using a column of chelating Sepharose Fast Flow (GE Healthcare Bio-Sciences Corp.) charged with Ni^{2+}. The N-terminal His tags were removed with thrombin (GE Healthcare Bio-Sciences Corp.) according to the manufacturer's instructions, and the proteins were purified to homogeneity on a Q Sepharose High Performance column (GE Healthcare Bio-Sciences Corp.).

Preparation of Metal-Reconstituted Wild-Type GKL and Its Mutants. Purified wild-type GKL and its mutants were dialyzed against storage buffer [100 mM NaCl and 20 mM Tris-HCl (pH 8.0)] containing 0.1 mM 2′-2-bipyridal, followed by dialysis in storage buffer to remove excess chelator. Metal-reconstituted GKL was prepared by dialysis of 2′-2-bipyridal-treated GKL against storage buffer containing 100 μM metal ions (Fe^{3+}, Zn^{2+}, Mn^{2+}, or combinations of two metals), followed by dialysis in storage buffer to remove unbound metal ions, before inductively coupled plasma optical emission spectroscopy (ICP-OES) metal analysis at the Elemental Analysis Laboratory, Department of Chemistry, National University of Singapore.

Kinetic Assay of Lactonase Activities. The lactonase activity of GKL was assayed by a continuous spectrophotometric assay as previously described,[5] using a UV-2550 spectrophotometer (Shimadzu). Briefly, the assay (1 mL at 37 °C) contained GKL, 2.5 mM bicine buffer (pH 8.3), 0.08 mM cresol purple (577 nm; ε = 12500 M^{-1} cm^{-1}), 100 μM metal ion (Zn^{2+} or Mn^{2+}), and 0.025−5.0 mM AHL substrate (substrates were dissolved in DMSO, and regardless of substrate concentration, the final concentration of organic solvent DMSO was maintained at 1%). Initial rates (ν_o) were corrected for the background rate of spontaneous substrate hydrolysis in the absence of enzyme. The background rate of substrate nonenzymatic hydrolysis varies among different substrates and concentrations tested but is typically <30 milliabsorbance units per minute, and significantly below the observed catalytic rates. Kinetic parameters were determined by fitting the initial rates to the Michaelis−Menten equation using Enzfitter (Biosoft).

Electron Paramagnetic Resonance (EPR) Studies. Metal-reconstituted wild-type GKL (Zn^{2+}) and E101N (Zn^{2+} or Mn^{2+}) and E101G/R230C (Zn^{2+}) mutants were concentrated to 50 mg/mL, transferred to quartz EPR tubes, and flash-frozen in liquid nitrogen. The continuous-wave EPR measurements were performed using an X-band (~9.05 GHz) Varian E-line 12″ spectrometer, equipped with a rectangular TM110 resonator and a helium cryostat. The microwave frequency and magnetic field were measured using the Varian internal frequency meter and field controller, respectively. Spectra were recorded at 10 and 60 K. Different modulation amplitudes between 0.1 and 1.0 mT were used to detect the signal of the paramagnetic centers unambiguously. The microwave power was between 0.2 and 2 mW to prevent signal saturation.

Crystallization and Data Collection. Frozen stocks of wild-type GKL and mutants were diluted to 50 mg/mL with their storage buffers, and C4-HSL was added to the catalytically inactive D266N mutants to a final concentration of 1.0 mM. Crystals grew within 2 weeks at 20 °C by the sitting-drop vapor diffusion method from a 1:1 (v/v) mixture with precipitant solution comprised of 100 mM Tris (pH 7.5), 20% (w/v) PEG 4000, 10% (v/v) glycerol, and 100 μM $ZnCl_2$ or $MnCl_2$. Crystals were harvested from the drop and directly flash-frozen in liquid nitrogen. X-ray diffraction data were collected at beamline BL13B1 on an Area Detection System Corp. Quantum-315 CCD detector at the National Synchrotron Research Center (Hsinchu, China), with different wavelengths (as summarized in Table 2) and a constant temperature at 105 K. Data were indexed, scaled, and merged in HKL2000.[8]

Structure Determination and Refinement. Structural determination was initiated by molecular replacement using the GKL D266N mutant [Protein Data Bank (PDB) entry 3OJG] as a model in PHASER.[9] The solution was subjected to repetitive rounds of restrained refinement in PHENIX[10] and manual building in COOT.[11] The C4-HSL ligand was then placed into the density in the active sites. The occupancies of the atoms in the ligand were refined as a group, while those of the two metal ions at the active site were refined individually. The chemical nature of the two metal ions was identified with the anomalous X-ray fluorescence method.[12] TLS parameters generated by the TLSMD web server[13] were included in the final round of refinement. The CCP4 program suite[14] was used for coordinate manipulations. The structures were validated with Molprobity.[15] All the structure-related figures were prepared with the PyMOL Molecular Graphics System (DeLano Scientific LLC).

RESULTS

Previously, we have determined that wild-type GKL is a metal-dependent quorum-quenching lactonase with an iron−zinc binuclear metal center within the active site.[3] 2′-2-Bipyridal-treated GKL was found to contain 0.1 equiv of iron and <0.01 equiv of zinc per active site. 2′-2-Bipyridal-treated GKL, like non-2′-2-bipyridal-treated GKL, did not have any detectable lactonase activity when assayed in the absence of additional metal ions. GKL exhibited detectable lactonase activity only when reconstitution was conducted with both Fe^{3+} and Zn^{2+}. Metal-reconstituted GKL contained 1.0 equiv of iron and 1.1 equiv of zinc per active site.

Table 1. Kinetic Parameters of GKL and Its Evolved Mutants

	GKL			E101G/R230C			R230D		
substrate	k_{cat} (s^{-1})	K_M (mM)	k_{cat}/K_M (M^{-1} s^{-1})	k_{cat} (s^{-1})	K_M (mM)	k_{cat}/K_M (M^{-1} s^{-1})	k_{cat} (s^{-1})	K_M (mM)	k_{cat}/K_M (M^{-1} s^{-1})
C4-HSL	ND[a]	ND[a]	ND[a]	≤0.010	*b*	*b*	ND[a]	ND[a]	ND[a]
3-oxo-C6-HSL	*c*	*c*	4.0	1.1 ± 0.32	22 ± 12	50	ND[a]	ND[a]	ND[a]
3-oxo-C8-HSL	0.21 ± 0.10	5.5 ± 2.1	38	2.1 ± 0.07	3.0 ± 0.4	700	≤0.026	*b*	*b*

	E101N (Zn^{2+}-reconstituted)			E101N (Mn^{2+}-reconstituted)		
substrate	k_{cat} (s^{-1})	K_M (mM)	k_{cat}/K_M (M^{-1} s^{-1})	k_{cat} (s^{-1})	K_M (mM)	k_{cat}/K_M (M^{-1} s^{-1})
C4-HSL	ND[a]	ND[a]	ND[a]	≤0.018	*b*	*b*
3-Oxo-C6-HSL	ND[a]	ND[a]	ND[a]	*c*	*c*	5.3
3-Oxo-C8-HSL	≤0.019	*b*	*b*	0.21 ± 0.11	4.0 ± 3.2	53

[a]No detectable activity. [b]Apparent k_{cat}. [c]Saturation kinetics could not be attained.

Table 2. Data Collection, Refinement, and Structure Validation Statistics[a]

	wild type	E101G/R230C	E101G/R230C/D266N	E101N	E101N	E101N/D266N	R230D
PDB entry	4H9U	4H9V	4H9X	4H9Y	4H9Z	4H9T	4HA0
metal	Zn	Zn	Zn	Zn	Mn	Mn	Zn
ligand			HL4			HL4	
			Data Collection				
space group	*P*1211	*P*1211	*P*1211	*P*1211	*P*1211	*P*212121	*P*22121
cell dimensions							
a, *b*, *c* (Å)	47.3, 157.1, 49.9	51.3, 130.2, 51.3	51.6, 129.2, 51.6	51.5, 128.5, 51.5	51.2, 127.8, 51.5	78.2, 91.4, 95.7	70, 76.2, 134.8
α, *β*, *γ* (deg)	90, 116.2, 90	90, 96.3, 90	90, 95.8, 90	90, 95.8, 90	90, 95.3, 90	90, 90, 90	90, 90, 90
resolution (Å)	30−2.10	50−1.97	50−2.20	50−2.09	30−2.60	30−2.10	30−1.90
I/σ	18.5 (2.6)	19.4 (3.8)	36.9 (3.8)	48.9 (6.0)	10.4 (3.7)	31.5 (3.7)	31.1 (3.5)
R_{merge} (%)	6.2 (41.8)	6.2 (22.0)	3.0 (27.3)	2.1 (16.6)	11.2 (21.5)	5.2 (44.3)	10.4 (40.6)
completeness (%)	98 (93)	92 (56)	99 (84)	97 (79)	89 (68)	100 (100)	98 (99)
redundancy	3.6 (3.0)	3.6 (2.9)	3.7 (2.9)	3.7 (3.2)	3.0 (2.4)	6.0 (5.3)	5.9 (5.9)
			Refinement				
resolution range (Å)	19.9−2.10	20.0−1.97	19.9−2.20	19.8−2.09	19.9−2.60	19.9−2.10	20.0−1.90
highest-resolution shell (Å)	2.16−2.10	2.02−1.97	2.27−2.20	2.14−2.08	2.74−2.60	2.15−2.10	1.93−1.90
no. of reflections	33812	38503	32403	38376	18030	40173	55872
completeness (%)	89 (37)	82 (33)	95 (60)	97 (80)	89 (56)	98 (80)	97 (98)
R_{work} (%)	17.5 (20.4)	18.5 (17.8)	17.8 (22.4)	19.2 (21.6)	18.7 (23.6)	19.1 (20.4)	26.1 (32.1)
R_{free} (%)	21.7 (26.6)	22.2 (23.8)	21.5 (31.7)	22.7 (25.8)	24.6 (29.5)	22.3 (25.2)	30.3 (37.2)
no. of atoms							
protein	5086	5014	5014	5024	5084	5034	5080
ion	6	6	6	6	4	6	6
ligand			24			24	
water	272	233	189	244	18	341	283
B factor (Å^2)							
protein	32.5	29.3	38.3	37.7	37.7	25.6	47.3
ion	17.2	17.9	28.3	31.5	26.4	29.4	32.0
ligand			53.4			43.1	
water	33.7	29.9	35.6	37.5	19.8	30.5	40.1
rmsd							
bonds (Å)	0.012	0.008	0.009	0.009	0.009	0.011	0.009
angles (deg)	1.288	1.102	1.174	1.162	1.162	1.263	1.194
			Molprobity Statistics				
all-atom clashscore	6.76	7.55	10.04	8.23	21.27	9.5	15.63
Ramachandran plot (%)							
outliers	0.2	0.0	0.2	0.0	0.2	0.0	0.0
allowed	2.3	2.6	2.1	2.6	5.1	1.9	2.7
favored	97.5	97.5	97.8	97.5	94.7	98.1	97.4
Rotamer outliers (%)	1.3	1.5	2.5	1.2	4.0	2.1	3.0
no. of C*β* deviations	1	1	0	0	0	0	1

[a]Values in parentheses are for the highest-resolution shell.

dx.doi.org/10.1021/bi4000904 | *Biochemistry* 2013, 52, 2359−2370

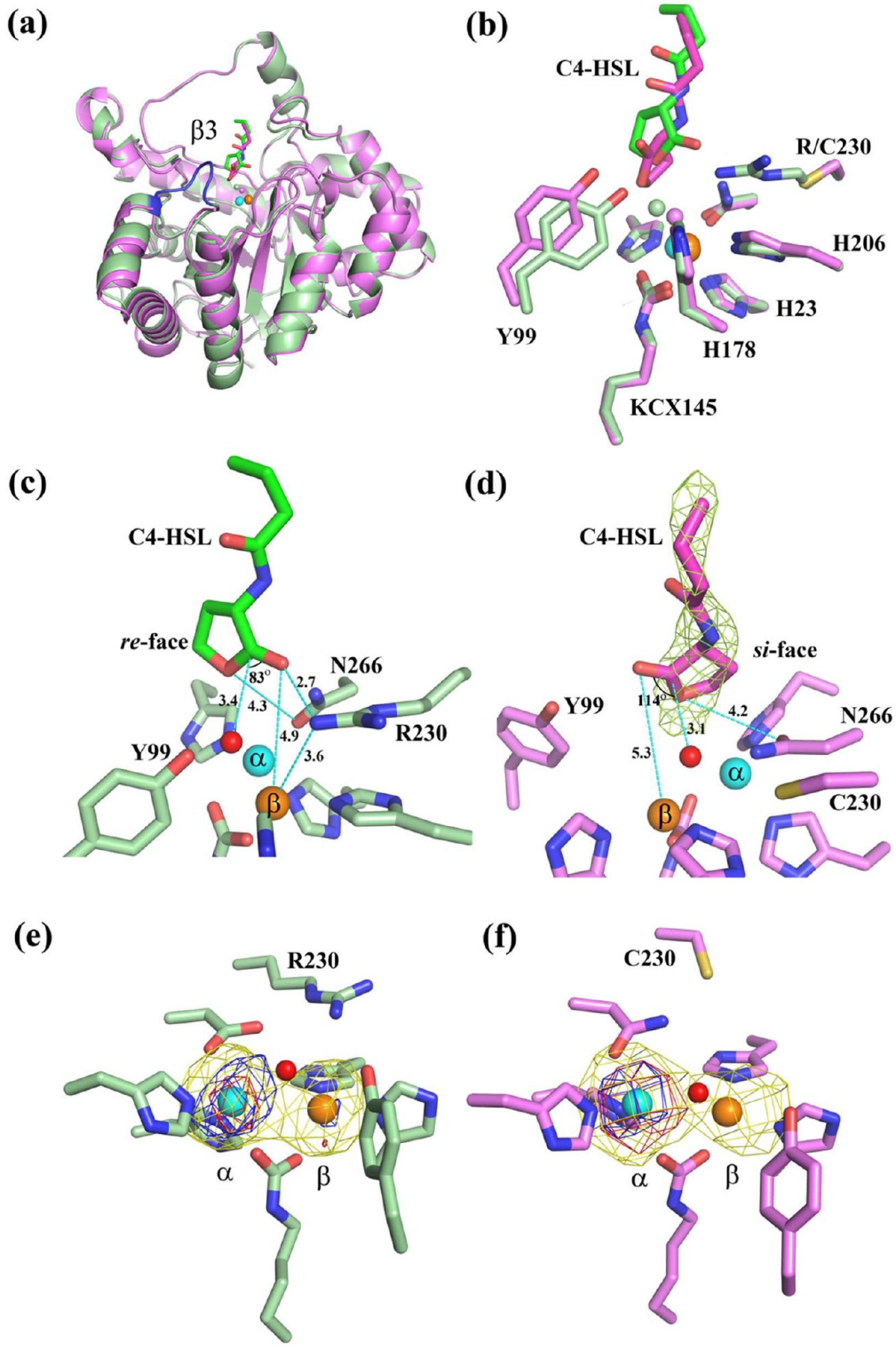

Figure 1. Structures of wild-type, E101G/R230C, and E101G/R230C/D266N GKL with bound C4-HSL. (a) Comparison between ligand-bound E101G/R230C/D266N and previously published D266N (PDB entry 3OJG), with D266N colored green and E101G/R230C/D266N colored magenta. The α-cation and the β-cation are depicted as cyan and orange spheres, respectively. The bridging hydroxide and the bound C4-HSL ligand are depicted as a sphere and sticks, respectively, with their colors following that of the peptide chain. The β3-loop in D266N is colored blue, which becomes disordered in E101G/R230C/D266N. (b) Close-up of the active site, highlighting changes in the bound ligand, and residues 99, 230, and 266. (c and d) Interatomic distances and facial selectivity in D266N (c) and E101G/R230C/D266N (d). The difference electron density map ($F_o - F_c$) in panel d, calculated by omitting the ligand and contoured at 3σ, is shown as a green mesh. (e and f) Bijvoet difference Fourier maps of wild-type GKL (e) and E101G/R230C (f) corresponding to data collected at 1.258 Å (yellow, with strong Zn fluorescence), 1.311 Å (red, without Zn fluorescence), 1.696 Å (blue, with strong Fe fluorescence), and 1.794 Å (no visible peak, without Fe fluorescence). All the maps are contoured at 3σ. These results clearly indicate that in both the wild type and E101G/R230C the α- and β-cation sites are mainly occupied by Fe and Zn ions, respectively.

dx.doi.org/10.1021/bi4000904 | *Biochemistry* 2013, 52, 2359−2370

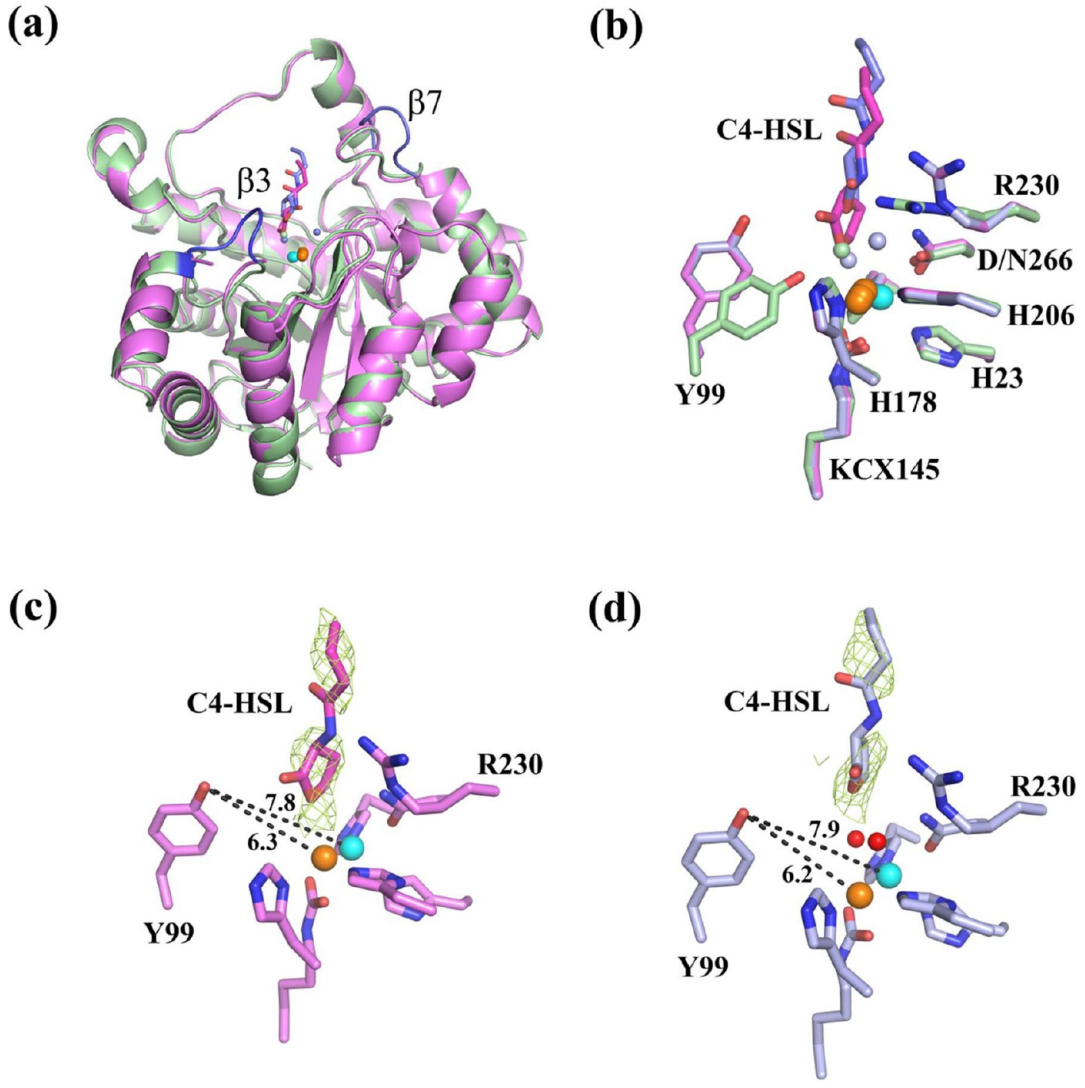

Figure 2. Structures of Mn^{2+}-reconstituted GKL mutants E101N and E101N/D266N with bound C4-HSL. (a) Overlay of chain A from ligand-free E101N (green) with the two chains from ligand-bound E101N/D266N. For the sake of clarity, the whole chain B of E101N/D266N is shown and colored magenta, while only the β7-loop and the bound ligand from chain A are shown and colored light blue. The α-cation and the β-cation are depicted as cyan and orange spheres, respectively. The ligand and water molecules near the active center are depicted as sticks and spheres, respectively, with their colors following that of the peptide chain. The β3-loop in E101N is colored blue. (b) Close-up of the active site, highlighting conformational changes in residues Tyr99 and Arg230, as well as the bound ligands. (c and d) Difference electron density map (green mesh) of the bound ligands in chains B (c) and A (d) of E101N/D266N. The maps are calculated by omitting the ligand and are contoured at 3σ.

Identification of a Mn^{2+}-Dependent GKL Mutant. When GKL mutants were screened for metal dependency, we identified a GKL mutant (E101N) that exhibited lactonase activity when reconstituted with manganese. Apart from E101N, other mutants of GKL (including the E101G/R230C mutant) exhibited detectable lactonase activity only upon reconstitution with zinc. In comparison to zinc-reconstituted E101N, the manganese-reconstituted E101N mutant exhibited greater lactonase activity against 3-oxo-C8-HSL and was able to hydrolyze 3-oxo-C6-HSL and C4-HSL when the zinc-reconstituted form could not (Table 1). Zinc-reconstituted E101N contained 1.0 equiv of iron and 1.1 equiv of zinc per active site, while manganese-reconstituted E101N contained 1.0 equiv of iron, 0.6 equiv of manganese, and 0.1 equiv of zinc per active site. Zinc-reconstituted E101G/R230C contained 0.9 equiv of iron and 1.0 equiv of zinc per active site.

Structures of GKL Mutants E101G/R230C and E101G/R230C/D266N with C4-HSL Ligands. Previously, we described the E101G/R230C mutant of GKL, obtained via directed evolution experiments, which had enhanced quorum-quenching activity.[3] This mutant exhibited a broadening of AHL substrate specificity (hydrolyzing C4-HSL, an AHL substrate that wild-type GKL did not hydrolyze) and increased catalytic activities against AHL substrates (kinetic parameters describing lactonase activities of wild-type and mutant GKL are detailed in Table 1). In an effort to obtain a structural explanation for the observed rate enhancements, we determined the structures of GKL mutant E101G/R230C, together with its catalytically inactive variant E101G/R230C/D266N with the quorum molecule C4-HSL bound in the active site. To facilitate the structural comparison and to determine the chemical nature of metal ions in the binuclear center, we also determined the wild-type GKL structure. The data processing and refinement statistics are listed in Table 2.

The overall structures of E101G/R230C, E101G/R230C/D266N with bound C4-HSL, and the wild type are similar to

dx.doi.org/10.1021/bi4000904 | *Biochemistry* 2013, 52, 2359−2370

Table 3. Color Properties and Active Site Architecture of Wild-type GKL and Its Mutants[a]

mutation (reconstitution)	absorbance maximum (nm)/molar extinction coefficient (M^{-1} cm^{-1})	color	β3-loop	distance (Å)			occupancy	
				$\alpha-\beta$	Y99–α	Y99–β	α	β
wild-type GKL (Fe^{3+}–Zn^{2+})	545/337	purple	ordered	3.6 (Fe–Zn)	6.2	4.6	1.0	1.0
E101G/R230C (Fe^{3+}–Zn^{2+})	512/376	purple	disordered	3.4 (Fe–Zn)	6.6	5.4	1.0	0.6
E101G/R230C/D266N (Fe^{3+}–Zn^{2+}) with C4-HSL	ND[b]	purple	disordered	3.6 (Fe–Zn)	7.2	5.6	1.0	0.7
E101N (Fe^{3+}–Zn^{2+})	535/435	dark brown	disordered	3.6 (Fe–Zn)	6.7	5.2	1.0	0.9
E101N (Fe^{3+}–Mn^{2+})	531/733	dark brown	ordered	3.2 (Fe–Mn)	4.8	2.9	1.0	1.0
E101N/D266N (Fe^{3+}–Mn^{2+}) with C4-HSL	ND[b]	dark brown	disordered	3.5 (Fe–Mn)	7.9	6.2	0.9	0.5
R230D (Fe^{3+}–Zn^{2+})	553/1066	dark purple	ordered	3.4 (Fe–Zn)	5.0	3.5	1.0	0.8

[a] α, α-cation; β, β-cation. [b] Not determined.

those of the previously reported D266N mutant of GKL[3] and organophosphorus hydrolase from *Geobacillus stearothermophilus* (PDB entry 3F4D).[16] The biological assembly is a dimer that occupies the asymmetric unit. A major difference lies in the β3-loop region, which is visible in the wild type and the D266N mutant, but becomes disordered in E101G/R230C and E101G/R230C/D266N. In both the D266N mutant and the wild type, the β3-loop is stabilized by the interaction between the side chain of Glu101 with those of Thr154 and Gln110. The E101G mutation abolishes these interactions, and hence, the loop is more mobile.

As observed in the D266N mutant, within the active site, which is located at the C-terminal end of the barrel, there are two metal ions bound at the α- and β-sites, corresponding to the more solvent-occluded and the more solvent-exposed cation positions, respectively. Using X-rays to scan for characteristic fluorescence absorption edges and inspection of anomalous difference Fourier electron density maps (together with ICP-OES and EPR data presented below), we have determined that the α-cation is occupied by Fe^{3+} and is coordinated by His23 and His25 at the end of the first β-strand, the carboxylated Lys145 at the end of the fourth β-strand, and Asp266 (Asn266 for the corresponding E101G/R230C/D266N GKL mutant) at the end of the eighth β-strand. The β-cation position is occupied by Zn^{2+} and is coordinated by His178 and His206 at the ends of the fifth and sixth β-strands, respectively, and by the carboxylated Lys145 at the end of the fourth β-strand. A bridging hydroxide ion serves as an additional ligand for both cations at approximately equal interatomic distances (Figure 1).

A change in the position and orientation of the bound C4-HSL becomes obvious when comparing E101G/R230C/D266N with previously published D266N. In E101G/R230C/D266N, the C4-HSL is positioned closer to the binuclear metal center, and the lactone ring is rotated by almost 90°. This change can be at least partly attributed to the R230C mutation. In the D266N mutant, the side chain of Arg230, which adopts the same conformation as in the wild type, is involved in positioning the bound C4-HSL by hydrogen bonding to the carbonyl oxygen on the lactone ring. With the loss of this interaction in E101G/R230C/D266N, the bound C4-HSL is less confined in its orientation. Consequently, the distances from the carbonyl carbon of the lactone ring to the attacking hydroxide nucleophile and the β-cation are both shortened (3.4 and 5.4 Å, respectively, in D266N vs 3.1 and 5.0 Å, respectively, in E101G/R230C/D266N), and the nucleophilic attack angle (between the nucleophile and the plane of the lactone ring formed by the carbonyl carbon and the oxo ring prior to the formation of the tetrahedral intermediate) changes from 28.9° in D266N to 51.0° in E101G/R230C/D266N.

Structure of GKL E101N Mutants and Mn^{2+}-Reconstituted E101N/D266N with C4-HSL. The Mn^{2+}-reconstituted E101N mutant of GKL exhibited enhanced quorum-quenching activity compared to that of wild-type GKL; this mutant, like the E101G/R230C mutant, exhibited a broadening of AHL substrate specificity, hydrolyzing C4-HSL, an AHL substrate that wild-type GKL did not hydrolyze. To elucidate the observed enhanced quorum-quenching activity, we determined the structures of both Mn^{2+}- and Zn^{2+}-reconstituted E101N, and Mn^{2+}-reconstituted, catalytically inactive mutant E101N/D266N with bound C4-HSL (Figure 2). Overall, these structures are similar to the other structures reported in this study. Similar to the E101G mutation, replacing Glu101 in the β3-loop with Asn increases the mobility of this loop in the Zn^{2+}-reconstituted E101N, rendering it invisible in the electron density maps. Interestingly, the same loop becomes ordered in Mn^{2+}-reconstituted E101N but regains its mobility when C4-HSL is bound, as observed in the structure of Mn^{2+}-reconstituted E101N/D266N with bound C4-HSL. A closer look at the binuclear center of Mn^{2+}-reconstituted E101N reveals dramatic changes in metal coordination. When Zn^{2+} occupies the β-cation position, the bridging hydroxide is approximately equidistant (2.2–2.6 Å) from the two metal ions, while in Mn^{2+}-reconstituted E101N, it resides 2.9 and 3.5 Å from the α- and β-cation, respectively. Furthermore, the side chain of Tyr99 moves closer to the β-cation, with a distance of 2.9 Å between the hydroxyl oxygen of Tyr99 and the Mn^{2+} (Table 3). Upon C4-HSL binding, this distance becomes 6.3 Å, as seen in E101N/D266N with bound C4-HSL.

The two monomers within the dimeric biological assembly are almost identical in all the structures reported here, except for Mn^{2+}-reconstituted E101N/D266N with bound C4-HSL, where the β7-loop adopts two different conformations, a "closed" conformation that is seen in most of the structures and an "open" conformation that is unique to one of the monomers. Correspondingly, the bound C4-HSL in the monomer with the closed β7-loop resembles that in E101G/R230C/D266N, while the substrate in the monomer with the open β7-loop is more

dx.doi.org/10.1021/bi4000904 | *Biochemistry* 2013, 52, 2359–2370

similar in conformation to the bound C4-HSL in D266N. Contrary to what is observed in the D266N mutant, and independent of the conformation of the β7-loop, the side chain of Arg230 adopts a conformation that is away from the binuclear center and does not have strong interaction with the carbonyl oxygen on the lactone ring of C4-HSL.

Charge Transfer in Wild-Type GKL and Its Mutants. Wild-type GKL and its mutants exhibited intense coloration at a high concentration (approximately 50 mg/mL).[3] We previously attributed this phenomenon to a charge-transfer complex between the active site tyrosine (Tyr99) and the bound iron (α-cation). This property was observed for Dr0930,[17] purple acid phosphatase,[18] and uteroferrin,[19] in which a charge-transfer complex between an active site tyrosine residue and the iron cation (in previously reported complexes) within the binuclear metal center was reportedly responsible for the observed purple coloration. In our attempts to arrive at a structural explanation for the observed charge-transfer complexes, the structure of GKL mutant R230D was determined in addition to the structures mentioned earlier. Wavelength scans of the various GKL mutants are presented in the Supporting Information.

A superposition of all the structures reveals remarkable (and expected) similarity in the overall structures. A close inspection of the active sites of the superposition, however, reveals significant perturbation to the position of the active site Tyr99 and, hence, to the overall geometry of the charge-transfer complex (Figure 3). As will be further discussed, mutations to amino acids 101 and 230, as well as substitution of zinc for manganese at the β-site, resulted in changes to the overall geometry of the active sites, contributing to the observed changes in the charge-transfer mutants. The properties of these charge-transfer mutants, including interatomic distances of the charge-transfer complexes, are listed in Table 3.

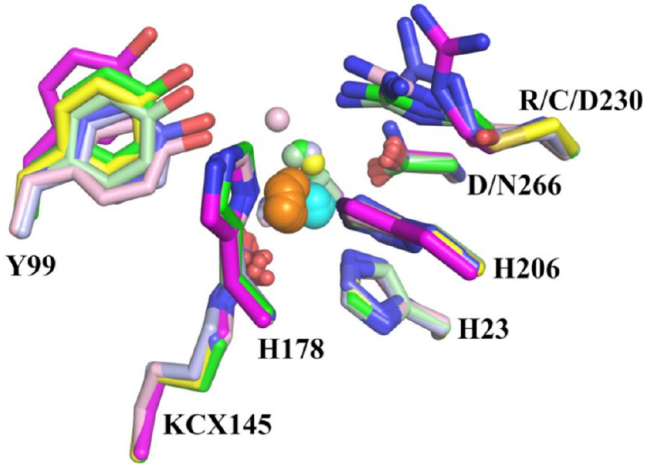

Figure 3. Superposition of the active sites of wild-type GKL (light green), E101G/R230C (yellow), E101N (green), R230D (light blue), Mn^{2+}-reconstituted E101N without (pink) and with (magenta) a bound ligand, and the hydrolase from *G. stearothermophilus* (blue, PDB entry 3F4D). The α-cation and the β-cation are depicted as cyan and orange spheres, respectively. Modulation of the charge-transfer complexes between Tyr99 and the β-cation is localized to the (re)positioning of Tyr99.

X-Band EPR Spectroscopy of Wild-Type GKL and Its Mutants. Frozen solutions of metal-reconstituted wild-type GKL (Zn^{2+}), E101N (Zn^{2+} or Mn^{2+}), and E101G/R230C (Zn^{2+}) mutants were studied by X-band EPR spectroscopy to ascertain the type and oxidation state of the metal ions in the respective binuclear centers. EPR spectra of Zn^{2+}-reconstituted wild-type GKL and its mutants (E101G/R230C and E101N) reveal an intense signal for a framework Fe^{3+} site with a $g = 4.3$ signal and several other much weaker signals (Figure 4). The position and shape of the $g = 4.3$ signal are characteristic of uncoupled, high-spin Fe^{3+} centers in rhombically distorted environments and for Fe^{3+} in binuclear $Fe^{3+}-Zn^{2+}$ centers,[20−23] and results from the $m_s = \pm^3/_2$ state. The minor $g \sim 5.2$ and 8.5 signals can be produced by the other state of the iron or cluster.[24] The weak resonances in the $g \sim 2.0-2.27$ area are also part of Fe^{3+} in a different environment (such as varying rhombic distortion within the binuclear center). The later resonances overlap with the multicomponent signal pertaining to Mn^{2+}. It is well observed in the Zn^{2+}-reconstituted samples of wild-type GKL and the E101N mutant (six lines with a splitting of ∼7.8−8.8 mT), but not the E101G/R230C mutant. We attribute this signal to "contaminating" Mn^{2+} in the β-site (we cannot rigorously exclude other metals, including Mn^{2+}, from our buffers; however, we have shown that wild-type GKL and its mutants, except E101N, are only active upon reconstitution with Zn^{2+}).

The spectrum of the Mn^{2+}-reconstituted E101N mutant of GKL also displayed the framework Fe^{3+} site signals (Figure 5). However, the shape of the line at $g = 4.3$ has changed and can be considered as a superposition of narrow and broad components. Another noteworthy peculiarity of this spectrum is the appearance of new intensive signals in the $g \sim 2.0$ area. The spectrum shows hyperfine structure consisting of ∼17 components with the ∼8.3 mT splittings at the low- and high-field edges. Six lines in the middle of the spectrum possess higher intensity and are indicative of the presence of Mn^{2+} (the six-line hyperfine structure is from ^{55}Mn with nuclear spin $I = {}^5/_2$). These six lines remained in the spectrum when the temperature was increased to 60 K, while other components of the hyperfine structure were not observed at this temperature. Our observations suggest that the multicomponent spectrum can be attributed to an overlap of the Mn^{2+} spectrum (six-line pattern) and the spectrum of the binuclear Mn cluster. Comparison of the hyperfine structure and total width of the cluster contribution to the spectrum with data available in the literature suggested a mixed-valence $Mn^{2+}-Mn^{3+}$ binuclear cluster.[25] In addition, the presence of a broad background line with a width of ∼200 mT may indicate the presence of a $Mn^{2+}-Mn^{2+}$ cluster in the sample.[26]

In summary, our EPR spectroscopy data suggest that upon Zn^{2+} or Mn^{2+} reconstitution, several types and combinations of mono- and dinuclear sites (including mixed and EPR-silent sites) may exist within the active sites of the respective wild-type and mutant GKL enzymes.

DISCUSSION

In our efforts to develop suitable antivirulence therapeutic agents for use in biomedical applications to address nosocomial bacterial infections, we obtained an in vitro evolved thermostable quorum-quenching lactonase (E101G/R230C mutant of GKL) that exhibited enhanced catalytic activities and broadened substrate range compared to those of the wild-type template.[3] The E101G/R230C mutant exhibited an increase in catalytic activity for AHL substrates; substrates tested include *N*-butyryl-DL-homoserine lactone (C4-HSL), *N*-hexanoyl-DL-homoserine lactone (C6-HSL), *N*-(3-oxohexano-

dx.doi.org/10.1021/bi4000904 | *Biochemistry* 2013, 52, 2359−2370

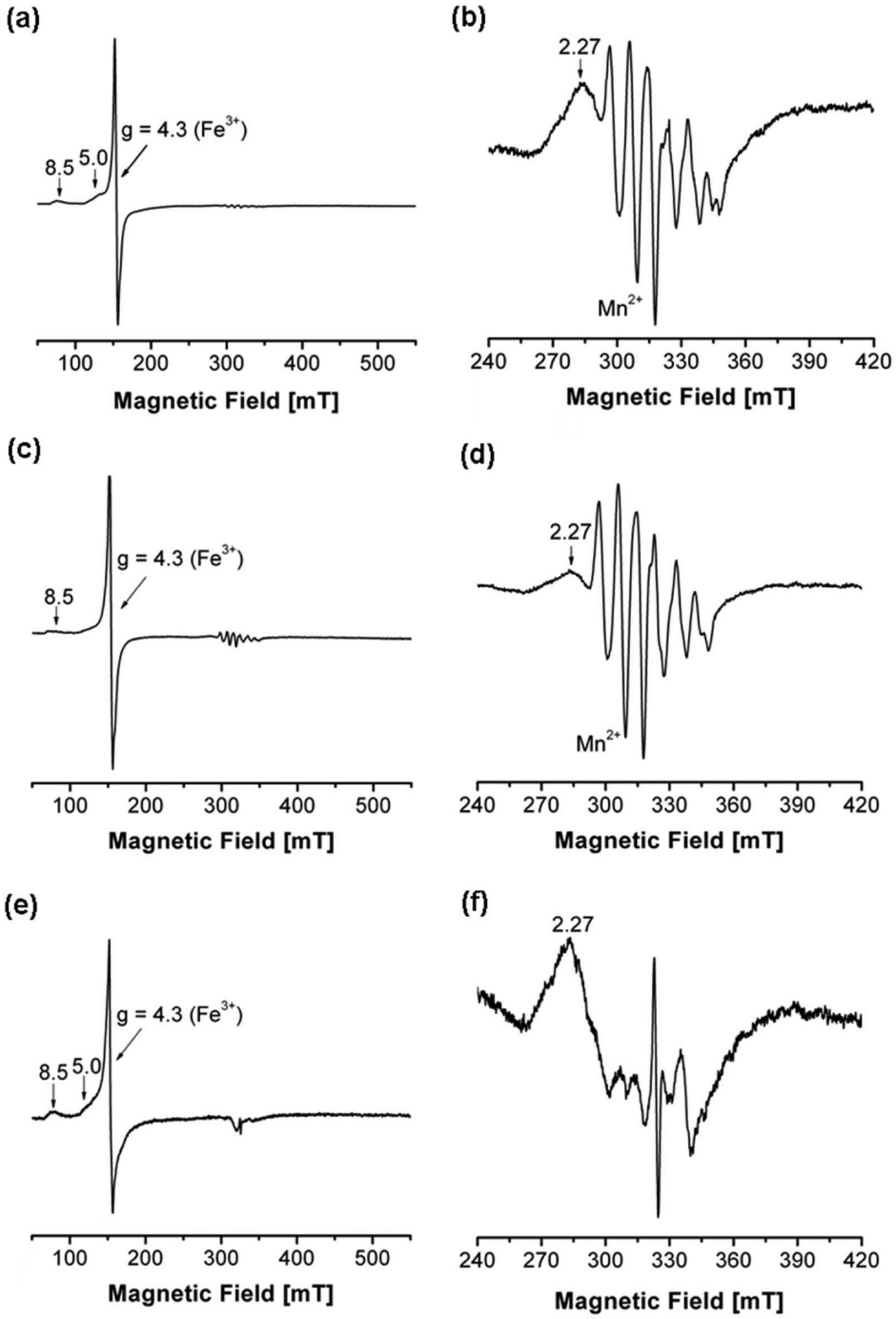

Figure 4. X-Band EPR spectra of Zn^{2+}-reconstituted wild-type GKL (a and b), the E101N GKL mutant (c and d), and the E101G/R230C GKL mutant (e and f) at temperatures of 11 (a and b) and 10 K (c–f); microwave frequencies of 9.0419 (a), 9.0459 (b), 9.0416 (c), 9.0444 (d), 9.0494 (e), and 9.0434 GHz (f), and a microwave power of 2 mW (a–f).

yl)-L-homoserine lactone (3-oxo-C6-HSL), *N*-octanoyl-DL-homoserine lactone (C8-HSL), *N*-(3-oxooctanoyl)-L-homoserine lactone (3-oxo-C8-HSL), and *N*-decanoyl-DL-homoserine lactone (C10-HSL). The chemical structures of these substrates are shown in Figure S1 of the Supporting Information. In comparison to wild-type GKL, this double mutant had increased k_{cat} values, decreased K_M values, and overall increases in catalytic efficiencies (k_{cat}/K_M) of 1.2-fold (for C6-HSL) to 32-fold (for 3-oxo-C12-HSL). Most noteworthy is the fact that the double mutation resulted in a broadening of AHL substrate specificity, allowing the quorum-quenching lactonase to hydrolyze C4-HSL, an AHL substrate that wild-type GKL did not previously hydrolyze. We sought to obtain a structural explanation for the observed enhanced reactivity of the E101G/R230C mutant to facilitate future catalytic design and engineering efforts.

EPR Spectroscopy of Wild-Type GKL and Its Mutants Identifies Different Types of Dinuclear Metal Sites. EPR spectroscopy can provide information about the type and oxidation state of paramagnetic metal ions as well as the spin coupling between metals in binuclear centers. For Zn^{2+}-reconstituted wild-type GKL and its mutants (including

dx.doi.org/10.1021/bi4000904 | *Biochemistry* 2013, 52, 2359–2370

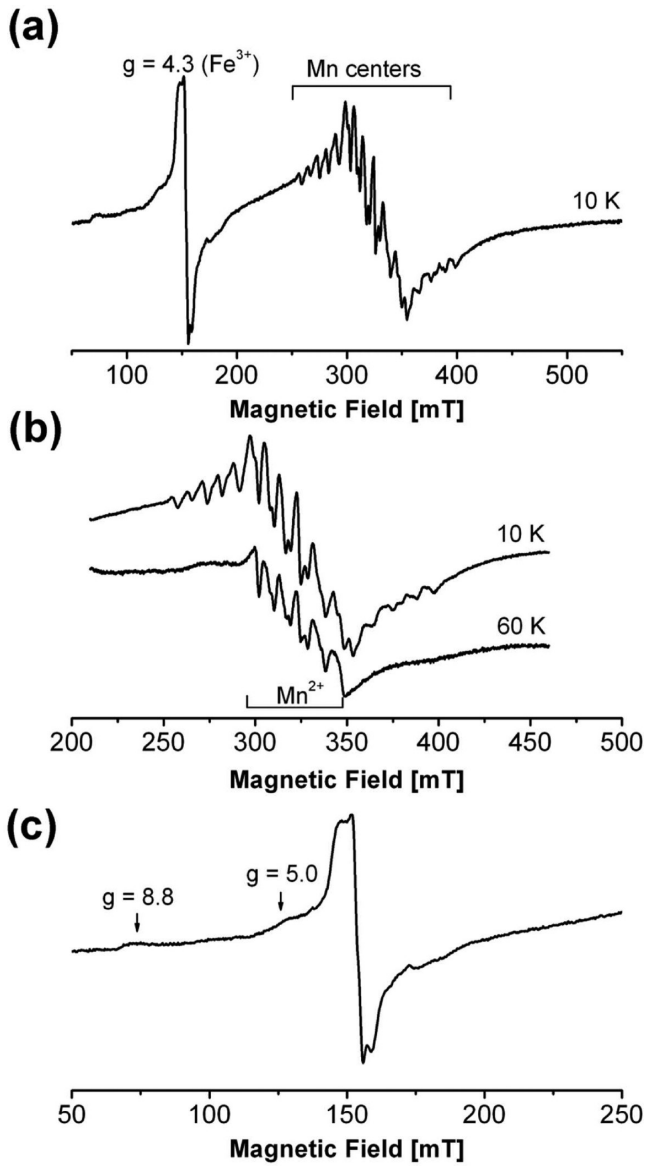

Figure 5. X-Band EPR spectrum of the Mn^{2+}-reconstituted E101N mutant of GKL (a), with high-field (b) and low-field (c) parts of this spectrum, at temperatures of 10 and 60 K, microwave frequencies of 9.0423 GHz at 10 K and 9.0414 GHz at 60 K, and a microwave power of 2 mW.

E101G/R230C), the α-cation position is occupied by high-spin Fe^{3+} while the β-cation position is presumably occupied by Zn^{2+} (we do not have "direct" EPR evidence as zinc is not paramagnetic), and not by another paramagnetic metal ion such as Mn^{2+}. Together with ICP-OES and EXAFS data, the binuclear active site of Zn^{2+}-reconstituted GKL enzymes is represented by a Fe^{3+}–Zn^{2+} center in the $S = {}^5/_2$ high-spin state, as illustrated in Figure 1. For the E101N–Mn mutant, our EPR data, in addition to high-spin Fe^{3+} state(s), reveal the presence of new spectra that could be assigned to Mn^{3+}–Mn^{2+} and Mn^{2+}–Mn^{2+} binuclear centers, based on previously reported studies of Mn–Mn binuclear centers in proteins and model complexes. The presence of the EPR silent, strongly antiferromagnetically coupled Fe^{3+}–Mn^{2+} center with $S = 0$[27] can also be suggested (and can be detected by other methods). Although the extent of the contribution of the respective Fe–Mn and Mn–Mn binuclear centers to activity is unclear, the fact remains that the effect of the E101N mutation, manifested through a change in the productive geometry of the charge-transfer complex, resulted in Mn^{2+}-dependent lactonase activity (a metal dependency not observed with wild-type GKL or with the evolved E101G/R230C mutant).

Structural Evidence of Rate Enhancement of Evolved GKL Mutants. The hydrolysis of AHL substrates by GKL is mediated by both the orientation of the substrate within the active site and the catalytic cycle that ensues: upon substrate binding, the carbonyl oxygen of the lactone ring would be polarized by interaction with the β-cation. A facial selectivity of the *re*-face of the lactone ring, consistent with observed facial orientations of the amide or ester bonds of substrates of other amidohydrolase superfamily members (such as dihydroorotase and isoaspartyl dipeptidase), would orient the scissile bond toward the hydroxide nucleophile that bridges the two metal ions. Nucleophilic attack by the bridging hydroxide would result in the formation of a tetrahedral intermediate, followed by the subsequent transfer of a proton from the hydroxide to Asp266, to yield the hydrolyzed acyl-homoserine, resulting in a quenching of quorum signaling.

The catalytic efficiency of the cycle is dependent on a number of factors, including (1) the ease of binding of the substrate within the active site, (2) the nucleophilicity of the bridging hydroxide, (3) the productive geometry presented within the active site architecture vis-à-vis the orientation of the scissile bond toward the attacking nucleophile, and (4) the resolution of the tetrahedral intermediate and subsequent ease of release of the product from the active site. Upon inspection of the pre-evolved GKL structure (represented by the C4-HSL-bound D266N GKL structure, PDB entry 3OJG), an explanation for the observed low catalytic AHL lactonase activities (or no detectable lactonase activity in the case of C4-HSL) is suggested. Successful formation of the tetrahedral intermediate during hydrolysis depends upon the productive geometry presented during nucleophilic attack; an efficient catalysis would involve an orthogonal (107°) angle of nucleophilic attack on the plane of the scissile bond.[28] In the case of wild-type GKL, the nucleophilic attack angle (represented by the angle formed by the nucleophile, the carbonyl C2 atom of the lactone ring, and the carbonyl O6 atom of the lactone) is 82.7°, a large deviation from the "perfect" orthogonal (107°) angle (Figure 1C); in addition, the position of the proposed nucleophile is almost in the plane of the lactone ring, and thus, the inability of wild-type GKL to hydrolyze C4-HSL is attributed to this unproductive geometry presented in the active site.

Previously, we proposed that the rate enhancements observed in AHL reactivity in the evolved mutant of GKL (we were unable to obtain suitable crystals of the E101N/R230I GKL mutant for structural studies; we report on the catalytically equivalent E101G/R230C GKL mutant in this study) could be attributed to the combined effects of an altered positioning of the lactone ring and a modulation of the attacking nucleophile toward the catalytically required and/or preferred orthogonal positioning to the scissile bond (Figure 1). An inspection of the evolved E101G/R230C mutant GKL structure (represented by the C4-HSL-bound E101G/R230C/D266N mutant GKL structure) corroborated the proposal for rate enhancement: an altered positioning of the lactone ring and a modulation of the position of the attacking hydroxide nucleophile led to an observed change in the nucleophilic attack angle of 114° (Figure 1D). Although this angle differs

dx.doi.org/10.1021/bi4000904 | *Biochemistry* 2013, 52, 2359–2370

from the orthogonal (107°) angle, it is considerably closer to the orthogonal angle, relative to the geometry presented in wild-type GKL! A superposition of the structure of the active E101G/R230C mutant with the inactive E101G/R230C/D266N mutant showed a virtually identical active site (rmsd of 0.248 Å); in addition, an observed modulation in the position of the proposed attacking nucleophile, from an almost in-plane position relative to the lactone ring (for wild-type GKL) to a more productive position of 51.0° relative to the plane of the lactone ring (for the evolved mutant), suggested that the observed C4-HSL-bound E101G/R230C/D266N mutant GKL structure is a good approximation of the evolved E101G/R230C mutant GKL structure.

A change in the facial selectivity of the lactone ring vis-à-vis orientation of the scissile bond toward the hydroxide nucleophile, from *re*-face (observed in wild-type GKL) to *si*-face (observed in the evolved E101G/R230C mutant), was noted (Figure 1). This facial selectivity is opposite to the observed facial orientations of the amide or ester bonds of substrates or inhibitors in the active sites of other amidohydrolase superfamily members such as dihydroorotase[29] and isoaspartyl dipeptidase.[30] Although we are unable to comment on the effect of facial selectivity on catalysis, we noticed that the E101G/R230C mutation caused a total translation of 79.9° (28.9° for the *re*-face and 51.0° for the *si*-face) for the attacking nucleophile, compared to wild-type (pre-evolved) GKL. A switch in the facial selectivity of the lactone ring was also observed for the catalytically competent Mn^{2+}-reconstituted E101N mutant of GKL (*si*-face, with an average angle of 29.1°).

On the basis of the work reported here and in our earlier paper,[3] as well as homologous structures[16,17,31] reported by others, a few key residues are highlighted. One such residue identified through random mutagenesis is Glu101, a residue remote from the active center.[3] As mentioned earlier, its side chain interacts with those of Gln110 and Thr154 from the same polypeptide chain. Substitution of this residue with Asn or Gly will abolish the former or both of these interactions, making the β3-loop more mobile, as evidenced by the absence of this loop in most of the structures bearing such mutations. The only exception observed so far is Mn^{2+}-reconstituted E101N, with the loop adopting the same conformation as in the wild type. However, this is accompanied by a much shorter distance between the hydroxyl group of Tyr99 and the β-cation. By considering all the data listed in Table 3, a coupling between this distance and the flexibility of the β3-loop is evident. The ordering of the β3-loop in Mn^{2+}-reconstituted E101N can thus be attributed to the tight tethering of Tyr99 by the β-cation, Mn^{2+} in this case, rather than the built-in stabilizing effect by Glu101, which it harbors.

Another key residue identified by our previously reported random mutagenesis approach is Arg230.[3] It has been shown previously that mutation at corresponding residues in some homologous proteins alters their enzymatic activities, such as the R228A mutation of Dr0930,[31] and the H254G mutation of phosphotriesterase.[32] In wild-type GKL, the side chain of Arg230 extends close to the active center, with its Nη2 atom sitting 3.8 Å from the β-cation, and forms a hydrogen bond to the catalytically critical residue Asp266 with its Nε atom (Figure 1). Arg230 is also involved in positioning the bound C4-HSL in an unfavorable orientation, which it does without needing to change the conformation, in the D266N mutant. These factors may contribute to wild-type GKL's nondetectable activity toward C4-HSL (Table 1). In contrast, in mutants that are active toward C4-HSL, this residue either is mutated, as in E101G/R230C (Figure 1) and E101N/R230I (no structure available), or moves away from the active center, as in Mn^{2+}-reconstituted E101N without or with bound C4-HSL (Figure 2). We can perceive that such changes would be beneficial to the enzyme's activity based on the catalysis mechanism mentioned earlier, where the β-cation polarizes the carbonyl oxygen of the lactone ring and makes the carbonyl carbon more susceptible to nucleophilic attack by the bridging hydroxide. Removing the side chain of Arg230, which acts as a hydrogen donor to Asp266 and probably an electron donor to the β-cation, from the active center would enhance the polarization effect of the β-cation on the carbonyl oxygen and promote the transfer of the proton from the bridging hydroxide to Asp266.

Tyr99 is the most perturbed residue at the active center (Figure 3). The distance between the hydroxyl group of Tyr99 and the β-cation depends on the chemical nature of the β-cation, the flexibility of the β3-loop next to Tyr99, and the presence or absence of the ligand at the active center (Table 3). A similar trend has been observed for the highly homologous Dr0930.[17,31] For the enzymatically active mutants, binding of C4-HSL invariably coincides with an increase in this characteristic distance, which is more pronounced when the β-cation position is occupied by Mn^{2+}. In analogy to the effect of the conformational change of Arg230, removal of the electron-rich hydroxyl group of Tyr99 from the β-cation would enhance its polarization effect on the carbonyl oxygen.

As has been clearly demonstrated (Table 1), the presence of the "correct" cation within the binuclear center is critical for the enzymatic activity of GKL toward AHL. A survey of homologous structures in the PDB reveals a common feature in that the occupancy of the two metal cations, especially that of the β-cation site, is less than unity, which is also the case for the structures reported here (Table 3). Interestingly, for the mutants that lose their Arg230, the occupancy of the β-cation is lower than the occupancy of those without such a mutation. Furthermore, among the ligand-free structures, the least occupied β-site is from the E101G/R230C mutant, which also has the largest distance between Tyr99 and the β-cation (Table 3). All these suggest that prior to ligand binding, both Arg230 and Tyr99 interact with the β-cation, acting as either sensors or determinants of the chemical nature and the occupancy of the β-cation.

Taken together, a structural explanation for the observed enzymatic activities of GKL and its mutants toward homoserine lactones can be drafted. In wild-type GKL, Arg230 makes the reaction less favorable by interacting with Asp266, the β-cation, and by positioning the ligand in a less optimal orientation. This effect can be alleviated by mutating this residue or by changing the chemical nature and occupancy of the β-cation. Another determinant for the enzymatic activity is the ease of movement of Tyr99 away from the β-cation, which is again affected by the identity and occupancy of the β-cation, as well as the flexibility of the adjacent β3-loop that in turn can be enhanced by mutating Glu101 within the loop. These two kinds of modulations are separately not sufficient for optimal enzymatic activities toward AHL, as manifested by the Zn^{2+}-reconstituted E101N or R230D mutant. When combined, however, they result in the enhanced activity of GKL, as exemplified by the E101G/R230C, E101N/R230I, and Mn^{2+}-reconstituted E101N mutants.

Although this study provides unequivocal evidence of a catalytically productive active site architecture of an evolved GKL that resulted in the observed increase in the level of catalysis, the exact nucleophilicity of the bridging and/or attacking hydroxide is still unclear and the extent of the contributions of the binuclear metal center on overall catalysis is still open to question. We are currently performing high-resolution EPR studies to obtain further insights into the role of the binuclear metal center (and the nucleophilicity of the attacking hydroxide) in catalysis.

Implications for Enzymatic Design and Catalysis. This study provides evidence that enhancement of enzyme activity can be caused by subtle (two point mutations), "remote" changes (Glu101 is located on a loop remote from the central catalytic barrel) that favor catalytically productive geometries during catalysis. The challenge in future catalytic design and engineering efforts will involve the incorporation of predictive algorithms into rational design protocols for fashioning suitable modulations of the active site architecture that take into account the productive geometries required for chemical catalysis.

■ ASSOCIATED CONTENT

Supporting Information

Chemical structures of various AHLs tested (Figure S1) and wavelength scans of wild-type GKL and its mutants (Figure S2). This material is available free of charge via the Internet at http://pubs.acs.org.

Accession Codes

The atomic coordinates and structure factors (PDB entries 4H9U, 4H9V, 4H9X, 4H9Y, 4H9Z, 4H9T, and 4HA0) have been deposited in the Protein Data Bank.

■ AUTHOR INFORMATION

Corresponding Author

*R.C.R.: telephone, 65-6586-9832; fax, 65-6779-1117; e-mail, rrobinson@imcb.a-star.edu.sg. W.S.Y.: telephone, 65-6516-8624; fax, 65-6779-1453; e-mail, bchyws@nus.edu.sg.

Author Contributions

B.X. and J.Y.C. contributed equally to this work.

Funding

This research was supported by grants from the National Medical Research Council and the National Research Foundation to W.S.Y., grants from the Biomedical Research Council of A*STAR to R.C.R., and National Institutes of Health Grant GM062954 and National Science Foundation Grant CHE-1026541 to S.A.D.

Notes

The authors declare no competing financial interest.

■ ACKNOWLEDGMENTS

We thank the National Synchrotron Radiation Research Center, a facility supported by the National Science Council of Taiwan, ROC, for provision of beam time and assistance in data collection. The Synchrotron Radiation Protein Crystallography Facility is supported by the National Research Program for Genomic Medicine.

■ ABBREVIATIONS

AHL, *N*-acyl-homoserine lactone; GKL, lactonase from *G. kaustophilus*; Dr0930, lactonase from *Deinococcus radiodurans*; IPTG, isopropyl D-thiogalactopyranoside; ICP-OES, inductively coupled plasma optical emission spectroscopy; EPR, electron paramagnetic resonance; rmsd, root-mean-square deviation.

■ REFERENCES

(1) Camilli, A., and Bassler, B. L. (2006) Bacterial small-molecule signaling pathways. *Science 311*, 1113−1116.

(2) Dong, Y. H., Wang, L. H., Xu, J. L., Zhang, H. B., Zhang, X. F., and Zhang, L. H. (2001) Quenching quorum-sensing-dependent bacterial infection by an N-acyl homoserine lactonase. *Nature 411*, 813−817.

(3) Chow, J. Y., Xue, B., Lee, K. H., Tung, A., Wu, L., Robinson, R. C., and Yew, W. S. (2010) Directed evolution of a thermostable quorum-quenching lactonase from the amidohydrolase superfamily. *J. Biol. Chem. 285*, 40911−40920.

(4) Afriat, L., Roodveldt, C., Manco, G., and Tawfik, D. S. (2006) The latent promiscuity of newly identified microbial lactonases is linked to a recently diverged phosphotriesterase. *Biochemistry 45*, 13677−13686.

(5) Chow, J. Y., Wu, L., and Yew, W. S. (2009) Directed Evolution of a Quorum-Quenching Lactonase from *Mycobacterium avium* subsp. *paratuberculosis* K-10 in the Amidohydrolase Superfamily. *Biochemistry 48*, 4344−4353.

(6) Gerlt, J. A., and Raushel, F. M. (2003) Evolution of function in $(\beta/\alpha)_8$-barrel enzymes. *Curr. Opin. Chem. Biol. 7*, 252−264.

(7) Seibert, C. M., and Raushel, F. M. (2005) Structural and catalytic diversity within the amidohydrolase superfamily. *Biochemistry 44*, 6383−6391.

(8) Otwinowski, Z., and Minor, W. (1997) Processing of X-ray diffraction data collected in oscillation mode. *Methods Enzymol. 276*, 307−326.

(9) McCoy, A. J., Grosse-Kunstleve, R. W., Adams, P. D., Winn, M. D., Storoni, L. C., and Read, R. J. (2007) Phaser crystallographic software. *J. Appl. Crystallogr. 40*, 658−674.

(10) Adams, P. D., Afonine, P. V., Bunkoczi, G., Chen, V. B., Davis, I. W., Echols, N., Headd, J. J., Hung, L. W., Kapral, G. J., Grosse-Kunstleve, R. W., McCoy, A. J., Moriarty, N. W., Oeffner, R., Read, R. J., Richardson, D. C., Richardson, J. S., Terwilliger, T. C., and Zwart, P. H. (2010) PHENIX: A comprehensive Python-based system for macromolecular structure solution. *Acta Crystallogr. 66*, 213−221.

(11) Emsley, P., Lohkamp, B., Scott, W. G., and Cowtan, K. (2010) Features and development of Coot. *Acta Crystallogr. 66*, 486−501.

(12) Elias, M., Dupuy, J., Merone, L., Mandrich, L., Porzio, E., Moniot, S., Rochu, D., Lecomte, C., Rossi, M., Masson, P., Manco, G., and Chabriere, E. (2008) Structural basis for natural lactonase and promiscuous phosphotriesterase activities. *J. Mol. Biol. 379*, 1017−1028.

(13) Painter, J., and Merritt, E. A. (2006) TLSMD web server for the generation of multi-group TLS models. *J. Appl. Crystallogr. 39*, 109−111.

(14) Winn, M. D., Ballard, C. C., Cowtan, K. D., Dodson, E. J., Emsley, P., Evans, P. R., Keegan, R. M., Krissinel, E. B., Leslie, A. G., McCoy, A., McNicholas, S. J., Murshudov, G. N., Pannu, N. S., Potterton, E. A., Powell, H. R., Read, R. J., Vagin, A., and Wilson, K. S. (2011) Overview of the CCP4 suite and current developments. *Acta Crystallogr. D67*, 235−242.

(15) Chen, V. B., Arendall, W. B., III, Headd, J. J., Keedy, D. A., Immormino, R. M., Kapral, G. J., Murray, L. W., Richardson, J. S., and Richardson, D. C. (2010) MolProbity: All-atom structure validation for macromolecular crystallography. *Acta Crystallogr. D66*, 12−21.

(16) Hawwa, R., Aikens, J., Turner, R. J., Santarsiero, B. D., and Mesecar, A. D. (2009) Structural basis for thermostability revealed through the identification and characterization of a highly thermostable phosphotriesterase-like lactonase from *Geobacillus stearothermophilus*. *Arch. Biochem. Biophys. 488*, 109−120.

(17) Xiang, D. F., Kolb, P., Fedorov, A. A., Meier, M. M., Fedorov, L. V., Nguyen, T. T., Sterner, R., Almo, S. C., Shoichet, B. K., and Raushel, F. M. (2009) Functional annotation and three-dimensional structure of Dr0930 from *Deinococcus radiodurans*, a close relative of

phosphotriesterase in the amidohydrolase superfamily. *Biochemistry 48*, 2237−2247.
(18) Davis, J. C., and Averill, B. A. (1982) Evidence for a spin-coupled binuclear iron unit at the active site of the purple acid phosphatase from beef spleen. *Proc. Natl. Acad. Sci. U.S.A. 79*, 4623−4627.
(19) Pyrz, J. W., Sage, J. T., Debrunner, P. G., and Que, L., Jr. (1986) The interaction of phosphate with uteroferrin. Characterization of a reduced uteroferrin-phosphate complex. *J. Biol. Chem. 261*, 11015−11020.
(20) David, S. S., and Que, L. (1990) Anion binding to uteroferrin. Evidence for phosphate coordination to the iron(III) ion of the dinuclear active site and interaction with the hydroxo bridge. *J. Am. Chem. Soc. 112*, 6455−6463.
(21) Palmer, G. (1985) The electron paramagnetic resonance of metalloproteins. *Biochem. Soc. Trans. 13*, 548−560.
(22) Schilling, O., Wenzel, N., Naylor, M., Vogel, A., Crowder, M., Makaroff, C., and Meyer-Klaucke, W. (2003) Flexible metal binding of the metallo-β-lactamase domain: Glyoxalase II incorporates iron, manganese, and zinc in vivo. *Biochemistry 42*, 11777−11786.
(23) Yu, L., Haddy, A., and Rusnak, F. (1995) Evidence That Calcineurin Accommodates an Active Site Binuclear Metal Center. *J. Am. Chem. Soc. 117*, 10147−10148.
(24) Durmus, A., Eicken, C., Horst Sift, B., Kratel, A., Kappl, R., Hüttermann, J., and Krebs, B. (1999) The active site of purple acid phosphatase from sweet potatoes (*Ipomoea batatas*). *Eur. J. Biochem. 260*, 709−716.
(25) Pessiki, P. J., Khangulov, S. V., Ho, D. M., and Dismukes, G. C. (1994) Structural and Functional Models of the Dimanganese Catalase Enzymes. 2. Structure, Electrochemical, Redox, and EPR Properties. *J. Am. Chem. Soc. 116*, 891−897.
(26) Pessiki, P. J., and Dismukes, G. C. (1994) Structural and functional models of the dimanganese catalase enzymes. 3. Kinetics and mechanism of hydrogen peroxide dismutation. *J. Am. Chem. Soc. 116*, 898−903.
(27) Schenk, G., Boutchard, C. L., Carrington, L. E., Noble, C. J., Moubaraki, B., Murray, K. S., de Jersey, J., Hanson, G. R., and Hamilton, S. (2001) A Purple Acid Phosphatase from Sweet Potato Contains an Antiferromagnetically Coupled Binuclear Fe-Mn Center. *J. Biol. Chem. 276*, 19084−19088.
(28) Bürgi, H. B., Dunitz, J. D., Lehn, J. M., and Wipff, G. (1974) Stereochemistry of reaction paths at carbonyl centres. *Tetrahedron 30*, 1563−1572.
(29) Thoden, J. B., Phillips, G. N., Jr., Neal, T. M., Raushel, F. M., and Holden, H. M. (2001) Molecular structure of dihydroorotase: A paradigm for catalysis through the use of a binuclear metal center. *Biochemistry 40*, 6989−6997.
(30) Marti-Arbona, R., Fresquet, V., Thoden, J. B., Davis, M. L., Holden, H. M., and Raushel, F. M. (2005) Mechanism of the reaction catalyzed by isoaspartyl dipeptidase from *Escherichia coli*. *Biochemistry 44*, 7115−7124.
(31) Hawwa, R., Larsen, S. D., Ratia, K., and Mesecar, A. D. (2009) Structure-based and random mutagenesis approaches increase the organophosphate-degrading activity of a phosphotriesterase homologue from *Deinococcus radiodurans*. *J. Mol. Biol. 393*, 36−57.
(32) Hill, C. M., Li, W. S., Thoden, J. B., Holden, H. M., and Raushel, F. M. (2003) Enhanced degradation of chemical warfare agents through molecular engineering of the phosphotriesterase active site. *J. Am. Chem. Soc. 125*, 8990−8991.